The Influence of Cold Plastic Deformation on Passivity of Ti-6Al-4V Alloy Studied by Electrochemical and Local Probing Techniques

Davood Nakhaie, Ali Davoodi,‡,* and Gholam Reza Ebrahimi***

ABSTRACT

The influence of cold plastic deformation on passivity of Ti-6Al-4V alloy (UNS R56400) was investigated by means of potentiodynamic polarization, Mott-Schottky analysis, atomic force microscopy, and scanning Kelvin probe force microscopy. The results showed that the cold working increased the passive current density. Mott-Schottky analysis revealed the n-type semiconducting behavior of the passive film. The donor density of the passive film was declined by increasing the film formation potential. On the other hand, work hardening increased the density of defects within the passive film, regardless of the applied potential. The Volta potential maps showed that α phase possesses lower surface potential compared to the β, i.e., 38.6 mV. The plastic deformation decreased the surface potential of both phases; however, the relative nobility of the constituent phases had been slightly affected by cold working, i.e., 5 mV. The topographic results after immersion of the alloy in an aggressive acidic environment revealed that the Volta potential difference between α and β was sufficient to make α more vulnerable to corrosion attacks.

KEY WORDS: atomic force microscopy, cold working, Mott-Schottky analysis, scanning Kelvin probe force microscopy, Ti-6Al-4V alloy

Submitted for publication: May 31, 2015. Revised and accepted: October 18, 2015. Preprint available online: October 26, 2015, http://dx.doi.org/10.5006/1794.

‡ Corresponding author. E-mail: a.davodi@um.ac.ir.

* Metallurgical and Materials Engineering Department, Faculty of Engineering, Ferdowsi University of Mashhad, P.O. Box 91775-1111, Iran.

** Materials & Polymer Engineering Department, Faculty of Engineering, Hakim Sabzevari University, Sabzevar, P.O. Box 391, Iran.

(1) UNS numbers are listed in *Metals and Alloys in the Unified Numbering System*, published by the Society of Automotive Engineers (SAE International) and cosponsored by ASTM International.

INTRODUCTION

Unique properties of titanium and its alloys have made them a promising material for many applications from aerospace and chemical industries to medicine. Ti-6Al-4V alloy (UNS R56400)[(1)] is perhaps the most common type among the titanium alloys. This alloy, which comprises two constituent phases of α and β, possesses high yield and ultimate strength, high fatigue strength, and excellent corrosion resistance in many environments.[1]

Work hardening is one of the strengthening mechanisms used in a number of alloy systems, at which higher yield strength can be achieved through the cold-working process. Also, cold working has been used as a finishing process in many industrial applications. The cold plastic deformation generally accompanies microstructural changes like increasing dislocations density, introducing deformation bands, and twinning.[2-5] Furthermore, the influence of cold working on corrosion resistance of alloys is of importance. It was shown that cold plastic deformation affects the pitting corrosion resistance and passive behavior of stainless steels and titanium alloys.[6-9] The passivity, which plays an important role on corrosion resistance of metals and alloys, can be evaluated by several surface analytical techniques, together with electrochemical methods. Among the electrochemical techniques used to study the passivity, Mott-Schottky analysis has been used to investigate the electron behavior of passive film formed on iron,[10] carbon steel,[11] nickel,[12] stainless steels,[13-14] and titanium.[15]

ISSN 0010-9312 (print), 1938-159X (online)
16/000017/$5.00+$0.50/0

In order to study the influence of microstructure on the corrosion behavior of multi-phase alloys, scanning Kelvin probe force microscopy (SKPFM) has been progressively used to map the Volta potential distribution of alloys like aluminum alloys,[16] magnesium alloys,[17-18] and copper alloys.[19-20] Using this method, the relative nobility of microstructural constituents, as well as their topography, can be evaluated with a high lateral resolution. It has been shown that the corrosion resistance of metals is correspondingly related to the work function of the elements, which is defined as the critical energy required to remove an electron from the metal into the vacuum.[21-22] A linear relationship between the Volta potential and free corrosion potential of a series of elements has been found.[22] The correlation between the work function and the applied stress on the metal has been studied in some research. For U-bended 304 stainless steel (UNS S30400), it was found that compression stress (inside of the U-bend) and tension stress (outside of the U-bend) increases and decreases the Volta potential, respectively, compared to unstressed areas.[23] Moreover, it was revealed that the elastic compressive strain increases the work function, while the elastic tensile strain decreases the electron work function.[24] It has also been pointed out that applied stress increases the surface roughness because of formation of deformation bands,[25] which indirectly changes the work function. Therefore, the effect of cold plastic deformation on corrosion tendency of metals and alloys can be evaluated by using proper techniques, e.g., SKPFM.[23]

The influence of cold deformation on localized corrosion of stainless steels has been the subject of several research studies.[6-8,26-27] For titanium and its alloys, however, limited numbers of studies have been devoted to establishing correlation between the plastic deformation and the corrosion resistance.[9,28] In the present study, Mott-Schottky analysis, potentiodynamic polarization, and local probing techniques have been tailored to address the influence of cold plastic deformation on passive behavior of Ti-6Al-4V alloy.

EXPERIMENTAL PROCEDURES

The bulk chemical composition of commercial Ti-6Al-4V alloy used in this study and the mean value of the main elements of constituent phases were determined by quantitative energy dispersive x-ray spectroscopy (EDS) and are given in Table 1. The alloy was annealed at 1,050°C for 1 h in a vacuum furnace followed by furnace cooling. Cylindrical specimens, 9 mm in height and 6 mm in diameter, were machined from the annealed alloy. Specimens were subjected to cold compression test using a Zwick/Roell-250[†] machine at room temperature at a strain rate of 0.01 s^{-1} and at two true strains (ε) of 2% and 5%, which were calculated using the following equation:

[†] Trade name.

TABLE 1

Chemical Composition (in wt%) of Bulk Ti-6Al-4V Alloy and Constituent Phases Determined with EDS Analysis

	Al	V	Ti
Bulk Alloy	6.15	4.02	89.79
α	6.58	2.30	91.10
β	2.11	15.63	82.21

$$\varepsilon = \ln \frac{L_f}{L_0} \quad (1)$$

where L_f is the instantaneous length and L_0 is the original length of the specimen.

After the compression test, specimens were cut at the middle, perpendicular to the applied stress. One half was used for SKPFM investigations and the other half was used for electrochemical experiments. For microstructural examination, the annealed specimen was prepared using conventional metallography method. The microstructure was examined by scanning electron microscopy (SEM) equipped with EDS.

Electrochemical experiments were conducted using three-electrode techniques in a cell containing 0.15 M NaCl solution open to air at 25±1°C. A saturated calomel electrode (SCE) as the reference electrode and a platinum mesh as the counter electrode were used. Prior to each experiment, specimens were successively wet abraded with SiC emery papers up to 2,500 grit. To ensure the reproducibility of results, all electrochemical experiments were repeated at least five times at identical conditions. For each electrochemical experiment, a fresh electrolyte was prepared using analytical grade reagents. Potentiodynamic polarization was conducted after recording the open circuit potential for 60 min at potential scan rate of 1 mV/s. For Mott-Schottky analysis, the working electrodes were initially pretreated cathodically at −1,200 mV_{SCE} for 15 min to remove the air-formed oxide film on the surface. Then, the passive films were grown on the specimens' surface by polarization at three constant potentials of 500 mV_{SCE}, 750 mV_{SCE}, and 1,000 mV_{SCE} for 120 min. Capacitance measurements were performed by sweeping the applied potential in the negative direction from 1,000 mV_{SCE} to −1,000 mV_{SCE} at a frequency of 4 kHz with small-amplitude sinusoidal voltage perturbation of 10 mV. For pure titanium, it was observed that at frequencies higher than 3.5 kHz, the capacitance becomes constant.[15] Therefore, it was expected that at frequencies higher than 3.5 kHz the electrochemical impedance is predominantly capacitive and is independent of frequency. The potential sweep rate was 1 mV/s, which was sufficiently fast to ensure that the vacancy structure of the passive film was "frozen in."[12]

The Volta potential images were obtained using a commercial Solver NEXT[†] atomic force microscopy (AFM) instrument (NT-MDT) from the mirror-like as-polished surface. All mappings were acquired in the air

at 25±1°C under controlled relative humidity of 35±2%. The AFM tip was an n-type antimony doped silicon pyramid single crystal, which was coated by conductive PtIr (25 nm) and Cr adhesive layer (2.5 nm). The surface potential mapping was performed by using dual-scan mode. To avoid the influence of topographic features on the surface potential mapping, the tip was lifted to 40 nm to 60 nm (depending on the surface roughness) during the second pass of the scan. The Volta potentials were scanned with a pixel resolution of 256×256 and a scan frequency rate of 0.3 Hz. As the actual Volta potential is the inversion of measured potential difference determined via SKPFM,[21] all shown Volta potential images were inverted to obtain the right polarity of the measured potential maps.

RESULTS AND DISCUSSION

Microstructure

The SEM micrograph of the annealed Ti-6Al-4V alloy is shown in Figure 1. As can be seen, the microstructure consists of wide, plate-like α with intergranular β. Using MIP Microstructural Image Processing Software†, α/β proportion was determined as 78%/22%. The α phase comprised a hexagonal close-packed (HCP) crystal structure, while the β phase was body-centered cubic (bcc).[29] The microstructure of Ti-6Al-4V alloy, which mainly depends on the heat treatment history, has strong influence on both the mechanical properties[30] and the corrosion resistance[31-32] of the alloy. The ternary phase diagram of the Ti-Al-V system suggests that at 1,050°C, β is the stable phase. During cooling of the alloy from the annealing temperature, at β transus temperature α precipitated, which resulted in dual phase of α+β structure at room temperature. The microstructure presented in Figure 1, which is known as equiaxed microstructure,[29-33] was the result of slow cooling from the annealing temperature and is in agreement with those that have been observed by Chen and Tsai.[34]

The Effect of Cold Working on Passivity

The potentiodynamic polarization curves at different levels of cold working, obtained in 0.15 M NaCl solution, are shown in Figure 2. There was a linear kinetics region in all curves, comparable to activation-controlled kinetics, which was up to approximately 350 mV above the corrosion potential. It is evident that cold plastic deformation depressed the anodic Tafel slope. Moreover, all of the specimens showed a steady passive current density at higher potentials, which implies that the alloy was instinctively passive in spite of the linear region at low potentials.[32] The corrosion potential and the passive current density of the Ti-6Al-4V alloy respectively decreased and increased as a result of plastic deformation. It is believed that the increase of surface roughness and dislocation density

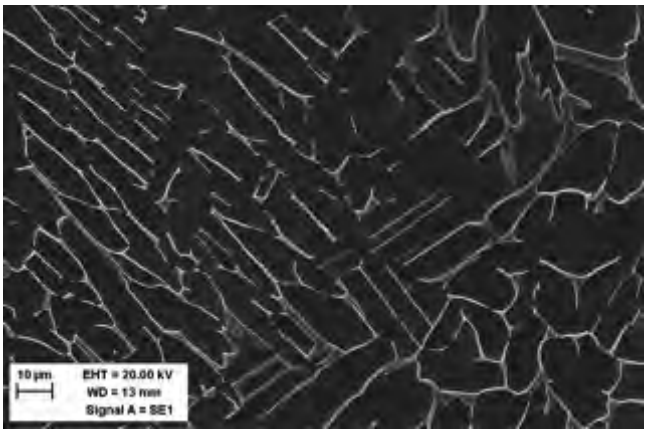

FIGURE 1. *SEM micrographs of solution-treated Ti-6Al-4V alloy.*

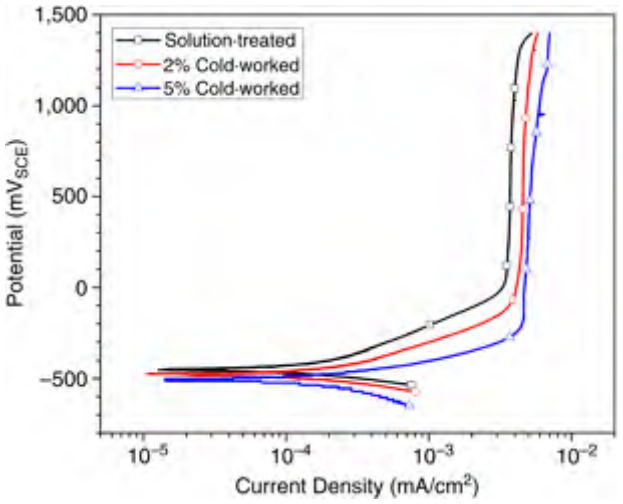

FIGURE 2. *Typical potentiodynamic polarization of Ti-6Al-4V for different levels of cold deformation obtained in 0.15 M NaCl solution at room temperature at potential scan rate of 1 mV/s.*

resulting from cold working influences the anodic dissolution of Ti alloy.[28] Similarly, for stainless steels, it was shown that the microstructural changes such as increasing the dislocations density, introducing deformation bands, and twinning during cold plastic deformation increased the passive current density.[6,26]

By measuring the capacitance of the space-charge region of a passive film as a function of the applied potential, the electronic properties of the passive film can be estimated. The capacitance of the film/electrolyte interface (C) is a combination of two capacitors in series, i.e., the double-layer capacitance (C_{dl}) and the space-charge capacitance (C_{sc}):

$$\frac{1}{C} = \frac{1}{C_{dl}} + \frac{1}{C_{sc}} \quad (2)$$

The interfacial capacitance is obtained from $C = 1/\omega Z''$, where ω is the angular frequency and Z″ is

the imaginary part of the impedance. It is reasonable to assume that at the passive film/electrolyte interface the capacitance of the double layer is considerably higher than that of the space-charge region; therefore, the former capacitance can be neglected. Consequently, the measured capacitance, C, during the Mott-Schottky analysis is equal to the space-charge capacitance. According to the Mott-Schottky theory,[35-36] the space-charge capacitance of an n-type semiconductor can be expressed as follow:

$$\frac{1}{C_{sc}^2} = \frac{2}{\varepsilon\varepsilon_0 e N_D}\left(V - V_{fb} - \frac{kT}{e}\right) \quad (3)$$

where ε is the dielectric constant of the oxide (proposed value of 80 for Ti-6Al-4V alloy[28]), ε_0 is the vacuum permittivity (8.85×10^{-14} F/cm), e is the charge of an electron (1.6×10^{-19} C), N_D is the donor concentration in the passive film, V denotes the applied potential, V_{fb} is the flat band potential, k is the Boltzmann constant (1.38×10^{-23} J/K), and T is the absolute temperature.

Figure 3 shows the Mott-Schottky plots for Ti-6Al-4V alloy in 0.15 M NaCl solution at 25°C as a function of cold plastic deformation. The plots were obtained after passive film growth at three distinct potentials of 500 mV_{SCE}, 750 mV_{SCE}, and 1,000 mV_{SCE} for 120 min. The positive slope of the Mott-Schottky plots is characteristic of the conductivity of an n-type semiconductor. The n-type character of the titanium oxide passive film was reported by others.[15,37] The n-type character of the titanium oxide implies that the main crystallographic defect in the passive layer is the oxygen vacancy and/or interstitial cation.[38] Because of the lower formation energy for an oxygen vacancy than titanium interstitial, it is highly likely that the donor species in Figure 3 is oxygen vacancy, which is the major anion vacancy in n-type oxide film such as the passive film on Ti.[15,39]

As depicted in Figure 3, the plastic deformation changed the electronic properties of the passive film. The donor level of the passive film as a function of cold plastic deformation was calculated for each film formation potential and presented in Figure 4. Each data point in Figure 4 represents the average donor density of the passive film calculated from five separate runs and the error bars show the 95% confidence limit. As can be seen, at constant film formation potential, by increasing the cold working, the density of defects increased, which implies that the crystal defects directly affect the electronic properties of the passive film formed on Ti alloy. Moreover, regardless of cold working, at higher film formation potentials the donor level of the oxide film decreased. The thickness and the composition of the oxide films formed by anodic polarization depended on the film formation potential.[37] The predominant oxide formed on Ti-6Al-4V alloy was TiO_2. Small amounts of Ti_2O_3 and TiO were also

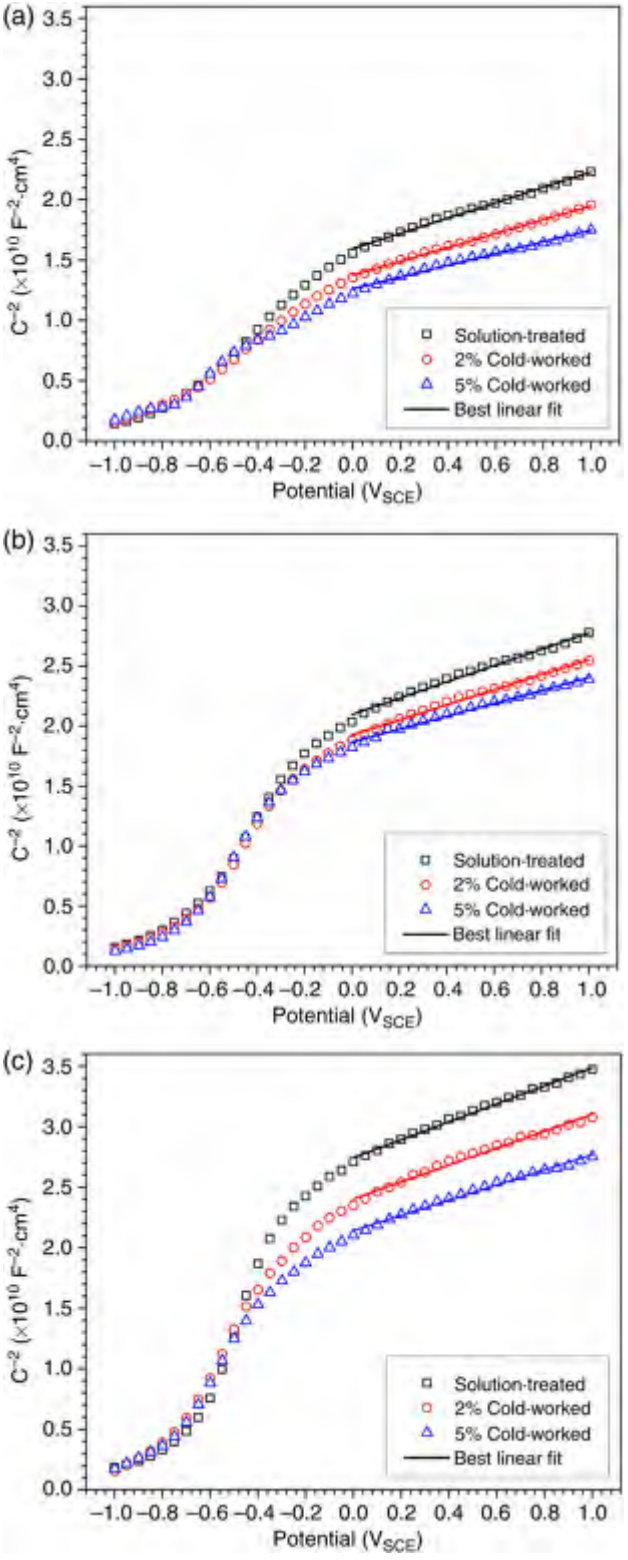

FIGURE 3. *Mott-Schottky plots for the passive film formed on Ti-6Al-4V with different cold-working levels. The film formation potentials were: (a) 500 mV_{SCE}, (b) 750 mV_{SCE}, and (c) 1,000 mV_{SCE}.*

detected at the metal/oxide interface. At the oxide/electrolyte interface, the oxide film is enriched with Al_2O_3.[40-43] It is believed that Ti oxide film possesses oxygen vacancies and an excess of metal ions.[37] Using

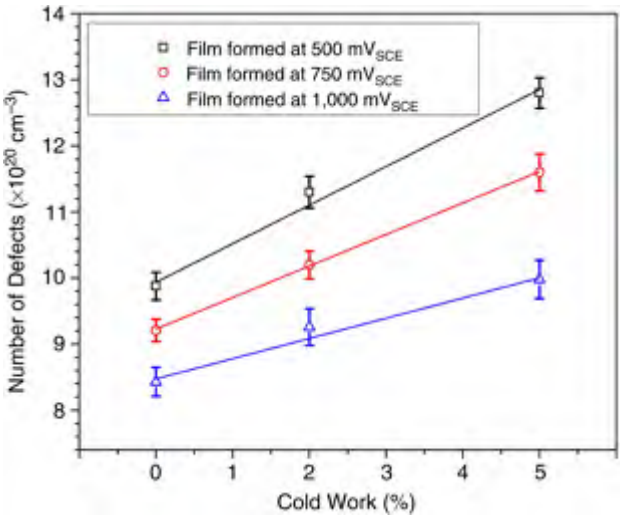

FIGURE 4. *Effects of film formation potential on the donor density for the passive film formed on Ti-6Al-4V as a function of cold plastic deformation in 0.15 M NaCl solution. The donor density was calculated from the linear slope of the Mott-Schottky plots presented in Figure 3. The error bars give the 95% confidence limit.*

x-ray photoelectron spectroscopy on anodically-formed oxide, it was confirmed that a metal surplus structure maybe attributed to Ti^{3+} ions. In order to attain electroneutrality, two Ti^{3+} ions in the oxide produce one oxygen vacancy. At higher oxidation potentials, the portion of Ti^{4+} in the passive film increases, while the Ti^{3+} content decreases. A reduced Ti^{3+} content in the passive film will result in fewer oxygen vacancies. Therefore, by increasing the film formation potential, the density of defects in the passive film decreases.[15] This behavior is true for both the solution-treated and the cold-worked specimens. Comparing three Mott-Schottky plots at each film formation potential, it is clear that the donor density of the passive film increased by increasing cold deformation. Thus, higher passive current density observed from the potentiodynamic polarization maybe ascribed to an increase in the donor density in the passive film.

Scanning Kelvin Probe Force Microscopy and Atomic Force Microscopy Investigations

Figure 5 presents the SKPFM images recorded on the as-polished surface of Ti-6Al-4V alloy at different levels of cold working. Regardless of the plastic deformation state, two distinct constituents on the alloy surface could be distinguished, i.e., a scattered bright region within a dark matrix. Comparing the Volta potential maps with the SEM micrograph (Figure 1), it is evident that the brighter phase, which possessed higher Volta potential, was β and the dark matrix with lower surface potential was α. The Volta potential difference between α and β has an important influence on corrosion susceptibility of these two constituent phases. As pointed out previously, the actual Volta potential map is the inverse of the recorded potential by

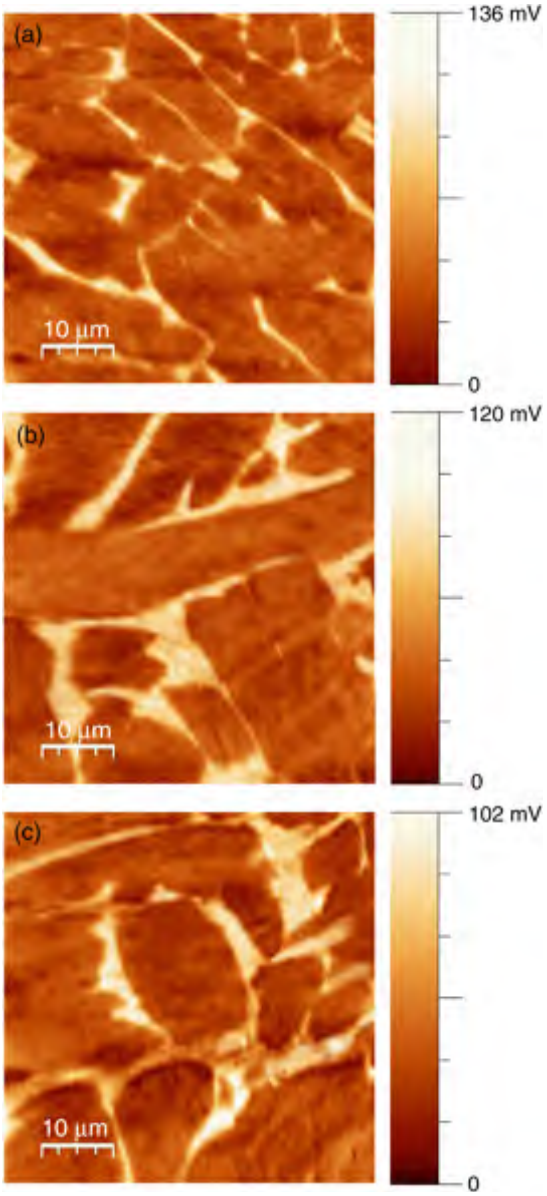

FIGURE 5. *Volta potential maps of: (a) solution-treated, (b) 2% cold-worked, and (c) 5% cold-worked. All Volta potential maps were obtained on as-polished surface.*

SKPFM. Therefore, all SKPFM images shown in Figure 5 are the inverse of the measured potential.

A common way to evaluate the Volta potential data is to use line profiles through the potential maps. Also, it has been shown that the Volta potential histogram provides broader information about the surface potential distribution.[19,44] The deconvolution of the Volta potential histograms into the multimodal Gaussian distributions were calculated using Equation (4) and are shown in Figure 6:

$$Y = \frac{1}{\sigma\sqrt{\pi/2}} \exp\left[-\frac{2(x-\mu)^2}{\sigma^2}\right] \quad (4)$$

TABLE 2

Extracted Multimodal Gaussian Distribution Parameters from the Volta Potential Histograms Represented in Figure 6

Specimen	Mean Potential Value, μ (mV)	Standard Deviation, σ (mV)	Driving Force, $\Delta\mu = \mu_{max} - \mu_{min}$ (mV)
Solution-Treated	$\mu_1 = 43.7$ $\mu_2 = 82.3$	$\sigma_1 = 19.5$ $\sigma_2 = 20.3$	38.6
2% Cold-Worked	$\mu_1 = 40.0$ $\mu_2 = 74.5$	$\sigma_1 = 23.5$ $\sigma_2 = 26.5$	34.5
5% Cold-Worked	$\mu_1 = 33.4$ $\mu_2 = 67.0$	$\sigma_1 = 23.2$ $\sigma_2 = 27.4$	33.6

where Y denotes the count number, σ is the standard deviation, μ is the mean value, and x is the Volta potential value. In order to quantitatively analyze the influence of cold plastic deformation on Volta potential distribution of Ti-6Al-4V alloy, three parameters were acquired from the deconvoluted histograms, i.e., the number of multimodal distribution peaks, the corresponding mean potential value (μ), and the standard deviation (σ). The extracted parameters are provided in Table 2. According to the Volta potential maps (Figure 5), β possesses higher surface potential than α. Therefore, the values of σ_1 and μ_1 correspond to α and σ_2, and μ_2 relate to β. As shown in Figure 6, there are two multimodal distribution peaks in each histogram. The difference between the mean potential values represents the driving force for microgalvanic localized corrosion. Moreover, the standard deviation gives the homogeneity of potential for a given constituent.[44] As can be seen from Table 2 and Figure 6, the cold plastic deformation decreased the mean potential value of both α and β. The galvanic driving force between two phases slightly decreased by cold working. Furthermore, the standard deviation of Volta potential distribution increased for work hardened specimens, which indicates that cold deformation increased the surface heterogeneity. The results summarized in Table 2 are in agreement with findings of other researchers,[23,25] who observed a decrease in Volta potential resulting from plastic deformation.

It has been shown that applied stress affects the work function of metals and alloys.[24-25,45] The work function is influenced by the cold deformation at two stages. During elastic tensile deformation, it is assumed that changing the distance between the surface atoms drops the potential across metal/vacuum interface, which decreases the work function, and hence, the Volta potential. On the contrary, elastic compression deformation increases the surface potential.[23] It has been found that in the plastic deformation stage the work function decreases.[25] The density of crystal defects (dislocations density in particular) increases as a result of work hardening of metals. Surface electrons are weakly bound, and because the plastic deformation

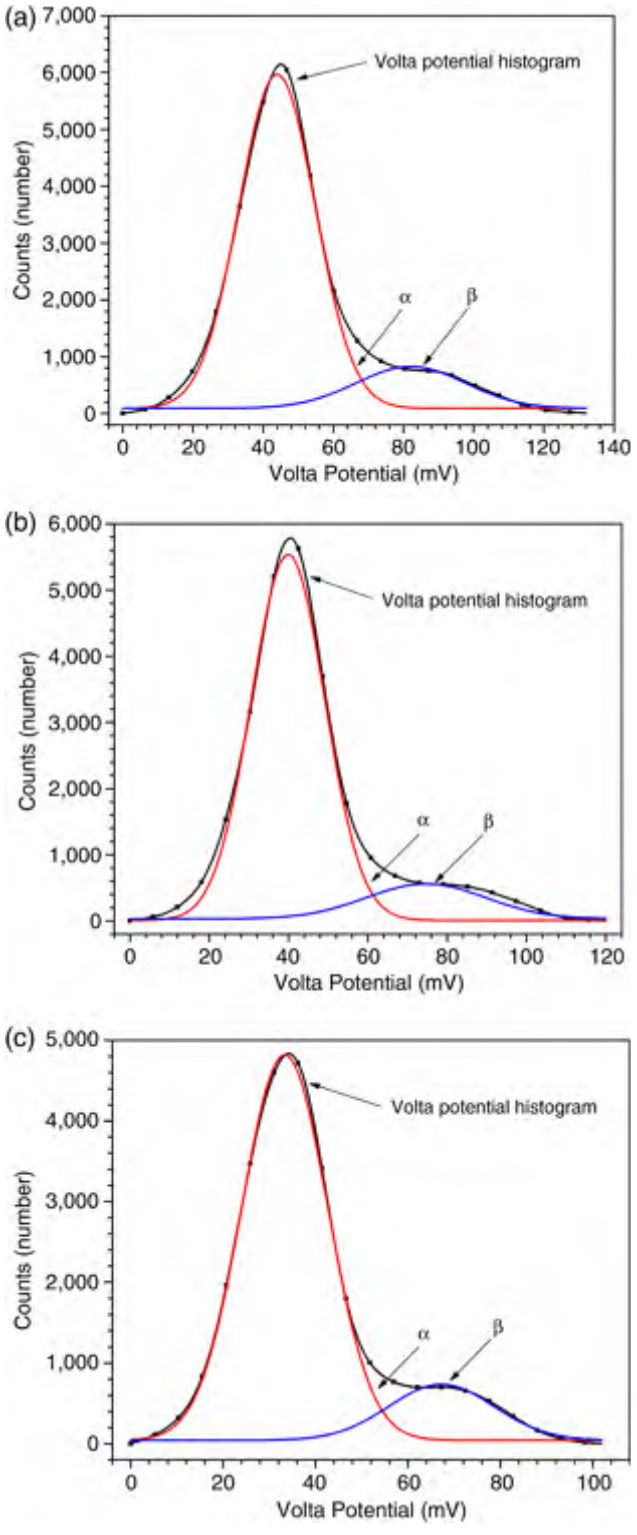

FIGURE 6. *Deconvoluted histogram of Volta potential map: (a) solution-treated, (b) 2% cold-worked, and (c) 5% cold-worked. The histograms represent simulated multimodal Gaussian distribution of Volta potential maps corresponding to Figure 5. Each peak represents the corresponding constituent phase, which is indicated based on the probabilities of Volta potential data.*

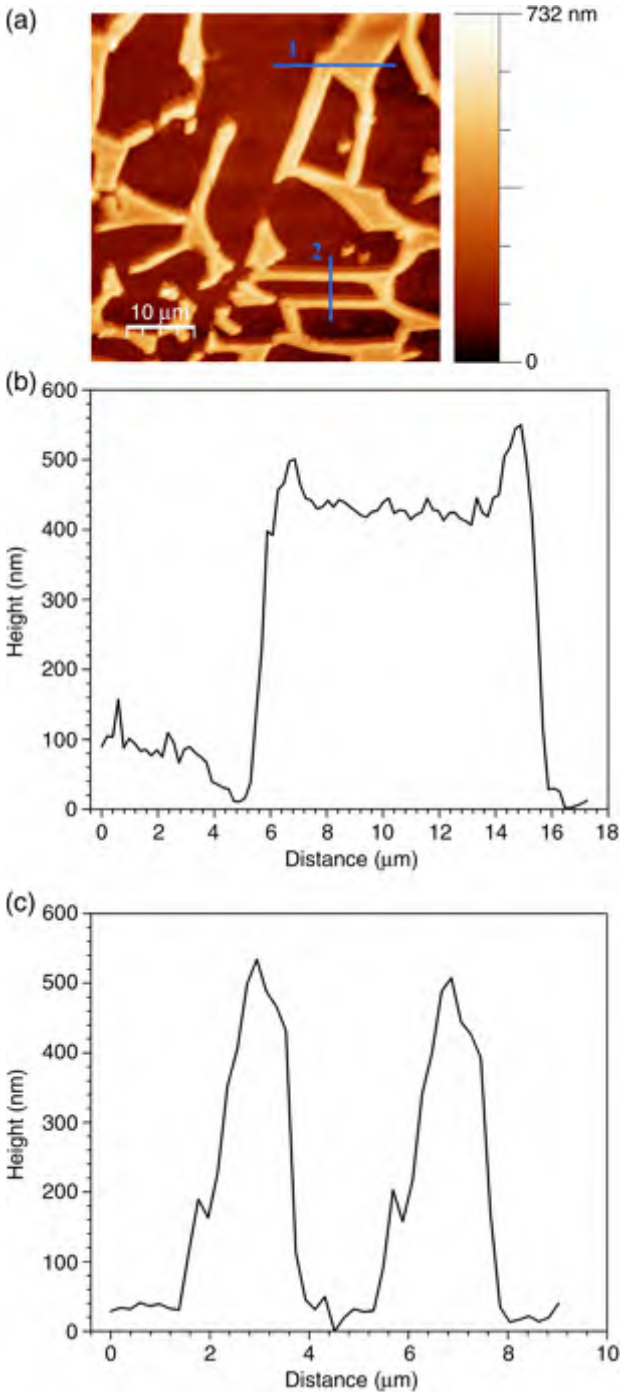

FIGURE 7. *(a) AFM topography image of the solution-treated Ti-6Al-4V alloy after immersion in 1 mL HF + 3 mL HNO_3 + 100 mL H_2O solution for 60 s, (b) corresponding height of line profile 1, and (c) corresponding height of line profile 2.*

increases the broken bonds as a result of increasing the density of crystal defects, therefore, surface electrons have more chances to escape from the surface. Consequently, according to the concept of the work function, the value of the work function for a work hardened metal decreases, which results in decrease in the surface potential.[23]

It is believed that in the plastic deformation stage dislocations are one of the main factors affecting the work function.[25] Furthermore, the value of work function is probably related to the dislocation multiplication, as well as to the formation of new surfaces. For an HCP metal like titanium, deformation twinning is an important deformation mode.[29] The twin volume fraction strongly depends on the grain size. However, it was shown that twinning contributes little to the plastic strain in the pure titanium.[4] The Ti-6Al-4V alloy comprises HCP α phase and bcc β phase. Deformation of α titanium takes place by slip and twinning, whereas plastic deformation in β titanium occurs by mechanisms typical of metals with bcc structure. Transmission electron microscopy (TEM) observations revealed that plastic deformation induces high density of dislocations.[3] Therefore, there is a good possibility that increasing the density of dislocations together with twinning (i.e., formation of new high energy surfaces) contributed to change in the work function of the cold deformed alloy in the present study. It was proposed that the dislocations generated because of plastic deformation increase the surface atomic roughness, vibration of the atoms, and consequently the surface entropy.[23] The jagged surfaces on metals show lower work functions than smooth surfaces.[24] However, the cold-worked specimens in the present study were polished after the plastic deformation. Therefore, the influence of surface roughness on Volta potential is negligible because deletion of the surface metal layer leads to a more uniform surface potential profile.

As mentioned previously, the Volta potential difference between constituent phases is an indication of the driving force for galvanic corrosion. The relative nobility of the microstructural constituents determines the preferential sites to onset the corrosion.[19,44] Therefore, besides the influence of plastic deformation on Volta potential distribution of individual phases, the relative nobility of α and β is of importance to evaluate the preferential sites for corrosion initiation. In the solution-treated condition, β showed higher surface potential than α. Such difference can be explained by the chemical composition of two phases. Using a simple linear equation proposed by Nakhaie, et al.,[19] the work function of individual microstructural constituents can be estimated:

$$W = \sum_i W_i \times a_i \quad (5)$$

where W is the work function of microstructural constituent, W_i is the work function of element i, obtained from Stanislaw and Tomasz,[45] and a_i is the atomic percent (at%) of element i. The values of the work function for α and β were calculated as 4.324 eV and 4.326 eV, respectively. The work function of β was just slightly higher than that of α. Even though the Volta potential difference between α and β was not

considerable, similar to those that have been reported for ferrite and austenite in duplex stainless steels for instance,[46-47] it was still enough to make α the preferential phase for corrosion attack to take place. By applying strain to the alloy, the mean value of Volta potential distribution of each phase decreased (up to 15 mV). However, the relative nobility of α and β remained nearly constant. A relatively larger effect (up to 200 mV) of the plastic deformation on the metal Volta potential has been observed.[23] It is assumed that the inconsistency can be attributed to the measuring method. Moreover, it is probable that higher plastic deformation may introduce more extensive effects on the Volta potential distribution. It is known that the relative nobility of the constituent phases determines the corrosion susceptibility;[19] therefore, it can be concluded that cold compression deformation up to 5% does not significantly alter the driving force for the microgalvanic corrosion of Ti-6Al-4V alloy. More deformation strain is probably required to enhance the differences.

Figure 7(a) shows the topography of solution-treated Ti-6Al-4V alloy after immersion in 1 mL HF + 3 mL HNO_3 + 100 mL H_2O solution for 60 s. In the topography image, the brightness of different zones equals to the difference in the heights of the features. The bright zones in the topographic image shown in Figure 7(a) are comparable with β phase, while the dark zones indicate α. As can be seen, the metal dissolution during immersion into the aggressive solution occurred faster in α. To investigate the dissolution of constituents in more details, two line profiles are presented in Figures 7(b) and (c). The line profiles clearly show that the corrosion attacks were considerably more intense in α than β. Higher dissolution rate in α phase than β on Ti-6Al-4V alloy surface is in agreement with the findings that were observed by using electrochemical AFM method.[34] The results obtained in the present study clearly show that in Ti-6Al-4V alloy comprised equiaxed microstructure, and given chemical composition, α is more vulnerable to corrosion than β. It is evident from topographic line profiles shown in Figures 7(b) and (c) that the maximum height regions corresponded to the boundary regions, which indicates the lowest dissolution area. Such step height between α and β phases has been also observed during immersion of Ti-6Al-4V alloy in acidic solution,[34] which may be attributed to partitioning of alloying elements at the phase boundaries. For a detailed explanation of the corrosion resistance of the phase boundaries, further studies are necessary, for instance using higher resolution SKPFM and TEM coupled with EDS.

CONCLUSIONS

❖ The influence of cold plastic deformation on passivity of Ti-6Al-4V alloy has been investigated using potentiodynamic polarization, Mott-Schottky analysis, SKPFM, and AFM techniques. Polarization experiments showed that the cold deformation decreased the corrosion potential, while the passive current density increased as a result of work hardening. From the Mott-Schottky analysis, it was found that the cold working increased the donor level of the oxide passive film. From the results obtained, it was established that the number of defects within the passive film was proportional to the bulk crystal defects of the alloy. Moreover, by increasing film formation potential, the density of defects declined, regardless of the cold-working level. SKPFM investigations revealed that α phase possesses lower Volta potential compared to β. Plastic deformation decreased the mean value of the surface potential of both α and β. However, the relative nobility difference of two constituents did not alter with cold working. Although the relative nobility of α and β was not substantial, it was still enough to make α more sensitive to corrosion attacks than β. Topography image after immersion into aggressive solution supported the SKPFM findings.

ACKNOWLEDGMENTS

Hakim Sabzevari University is acknowledged for providing the experimental facilities. The first author would like to express his gratitude to Mr. M. Makarem and NPD Co. for image processing.

REFERENCES

1. C. Leyens, M. Peters, *Titanium and Titanium Alloys: Fundamentals and Applications* (Weinheim, Germany: Wiley-VCH, 2003).
2. A.A. Salem, S.R. Kalidindi, R.D. Doherty, *Acta Mater.* 51 (2003): p. 4225.
3. D.G.L. Prakash, R. Ding, R.J. Moat, I. Jones, P.J. Withers, J.Q. da Fonseca, M. Preuss, *Mater. Sci. Eng. A* 527 (2010): p. 5734.
4. A. Ghaderi, M.R. Barnett, *Acta Mater.* 59 (2011): p. 7824.
5. F. Xu, X. Zhang, H. Ni, Q. Liu, *Mater. Sci. Eng. A* 541 (2012): p. 190.
6. A. Barbucci, G. Cerisola, P.L. Cabot, *J. Electrochem. Soc.* 149 (2002): p. B534.
7. U. Kamachi Mudali, P. Shankar, S. Ningshen, R.K. Dayal, H.S. Khatak, B. Raj, *Corros. Sci.* 44 (2002): p. 2183.
8. D. Nakhaie, M.H. Moayed, *Corros. Sci.* 80 (2014): p. 290.
9. H. Krawiec, V. Vignal, J. Loch, P. Erazmus-Vignal, *Corros. Sci.* 96 (2015): p. 160.
10. S.J. Ahn, H.S. Kwon, *Electrochim. Acta* 49 (2004): p. 3347.
11. Y.F. Cheng, C. Yang, J.L. Luo, *Thin Solid Films* 416 (2002): p. 169.
12. S. Ahn, H. Kwon, D.D. Macdonald, *J. Electrochem. Soc.* 152 (2005): p. B482.
13. Z. Feng, X. Cheng, C. Dong, L. Xu, X. Li, *Corros. Sci.* 52 (2010): p. 3646.
14. L.V. Taveira, M.F. Montemor, M. Da Cunha Belo, M.G. Ferreira, L.F.P. Dick, *Corros. Sci.* 52 (2010): p. 2813.
15. D. Sazou, K. Saltidou, M. Pagitsas, *Electrochim. Acta* 76 (2012): p. 48.
16. F.N. Afshar, A.M. Glenn, J.H.W. de Wit, H. Terryn, J.M.C. Mol, *Electrochim. Acta* 104 (2013): p. 48.
17. A.J. López, C. Taltavull, B. Torres, E. Otero, J. Rams, *Corrosion* 69 (2013): p. 497.
18. M.F. Hurley, C.M. Efaw, P.H. Davis, J.R. Croteau, E. Graugnard, N. Birbilis, *Corrosion* 71 (2015): p. 160.
19. D. Nakhaie, A. Davoodi, A. Imani, *Corros. Sci.* 80 (2014): p. 104.
20. Q.N. Song, Y.G. Zheng, D.R. Ni, Z.Y. Ma, *Corros. Sci.* 92 (2015): p. 95.

21. A.B. Cook, Z. Barrett, S.B. Lyon, H.N. McMurray, J. Walton, G. Williams, *Electrochim. Acta* 66 (2012): p. 100.
22. V. Guillaumin, P. Schmutz, G.S. Frankel, *J. Electrochem. Soc.* 148 (2001): p. B163.
23. A. Nazarov, D. Thierry, *Electrochim. Acta* 52 (2007): p. 7689.
24. V.V. Levitin, S.V. Loskutov, M.I. Pravda, B.A. Serpetzky, *Solid State Comm.* 92 (1994): p. 973.
25. W. Li, M. Cai, Y. Wang, S. Yu, *Scrip. Mater.* 54 (2006): p. 921.
26. G. Salvago, G. Fumagalli, D. Sinigaglia, *Corros. Sci.* 23 (1983): p. 515.
27. Y. Fu, X. Wu, E.-H. Han, W. Ke, K. Yang, Z. Jiang, *Electrochim. Acta* 54 (2009): p. 1618.
28. H. Krawiec, V. Vignal, E. Schwarzenboeck, J. Banas, *Electrochim. Acta* 104 (2013): p. 400.
29. M. Motyka, K. Kubiak, J. Sieniawski, W. Ziaja, "Phase Transformations and Characterization of α + β Titanium Alloys," in *Comprehensive Materials Processing*, ed. S. Hashmi (Oxford, United Kingdom: Elsevier, 2014), p. 7.
30. G.Q. Wu, C.L. Shi, W. Sha, A.X. Sha, H.R. Jiang, *Mater. Design* 46 (2013): p. 668.
31. M. Atapour, A. Pilchak, G.S. Frankel, J.C. Williams, *Corros. Sci.* 52 (2010): p. 3062.
32. M. Atapour, A. Pilchak, G.S. Frankel, J.C. Williams, M.H. Fathi, M. Shamanian, *Corrosion* 66 (2010): p. 065004-1.
33. R.J. Morrissey, D.L. McDowell, T. Nicholas, *Int. J. Fatigue* 21 (1999): p. 679.
34. J.-R. Chen, W.-T. Tsai, *Electrochim. Acta* 56 (2011): p. 1746.
35. N.B. Hakiki, S. Boudin, B. Rondot, M. Da Cunha Belo, *Corros. Sci.* 37 (1995): p. 1809.
36. N.E. Hakiki, M. Da Cunha Belo, A.M.P. Simões, M.G.S. Ferreira, *J. Electrochem. Soc.* 145 (1998): p. 3821.
37. M. Metikoš-Huković, A. Kwokal, J. Piljac, *Biomater.* 24 (2003): p. 3765.
38. D.D. Macdonald, S.R. Biaggio, H. Song, *J. Electrochem. Soc.* 139 (1992): p. 170.
39. Z. Jiang, X. Dai, T. Norby, H. Middleton, *Corros. Sci.* 53 (2011): p. 815.
40. M. Ask, J. Lausmaa, B. Kasemo, *Appl. Surf. Sci.* 35 (1989): p. 283.
41. R.N.S. Sodhi, A. Weninger, J.E. Davies, K. Sreenivas, *J. Vacuum Sci. Technol. A* 9 (1991): p. 1329.
42. I. Milošev, M. Metikoš-Huković, H.H. Strehblow, *Biomater.* 21 (2000): p. 2103.
43. L. Thair, U. Kamachi Mudali, S. Rajagopalan, R. Asokamani, B. Raj, *Corros. Sci.* 45 (2003): p. 1951.
44. M. Sarvghad-Moghaddam, R. Parvizi, A. Davoodi, M. Haddad-Sabzevar, A. Imani, *Corros. Sci.* 79 (2014): p. 148.
45. H. Stanislaw, D. Tomasz, *J. Physics: Condensed Matter* 10 (1998): p. 10815.
46. N. Sathirachinda, R. Pettersson, J. Pan, *Corros. Sci.* 51 (2009): p. 1850.
47. N. Sathirachinda, R. Pettersson, S. Wessman, J. Pan, *Corros. Sci.* 52 (2010): p. 179.